Langmuir
Letter

pubs.acs.org/Langmuir

Characterization of the Dominant Molecular Step Orientations on Hydroxyapatite (100) Surfaces

Ki-Young Kwon, Eddie Wang, Neil Chang, and Seung-Wuk Lee*

Department of Bioengineering, University of California, Berkeley, Physical Biosciences Division, Lawrence Berkeley National Laboratory, Berkeley Nanoscience and Nanoengineering Institute, Berkeley, California 94720

Received March 6, 2009. Revised Manuscript Received April 29, 2009

Hydroxyapatite (HAP) is the major inorganic component of bones and teeth. The characterization of HAP surfaces on the molecular level is important for achieving a fundamenatal understanding of bone remodeling and dental caries processes. On the microscopic level, hydroxyapatite growth and dissolution reactions mainly occur at steps. Therefore, this study focuses on individual molecular steps on HAP (100) facets under both static conditions and dynamic dissolution conditions using atomic force microscopy (AFM). We found that molecular steps parallel to the elongated axes of HAP crystals and those angled approximately 54° against the elongated axis are not only energetically favorable but also kinetically dominant under dissolution conditions.

Mature mammalian hard tissues are composed mainly of calcium phosphates in the form of mineralized biological apatites. Biological apatites vary in impurity content but are most closely related to hydroxyapatite (HAP), $Ca_{10}(PO_4)_6(OH)_2$.[1,2] Therefore, HAP is often used as a model for studying biological apatites. There have been tremendous efforts attempting to detail how various molecules interact with biologically derived and synthetic apatites in order to better understand their roles in hard tissue biomineralization and integrity.[3−7] For example, the molecular-level mechanisms through which bone- and tooth-associated proteins or macromolecules recognize HAP surfaces have been studied using solid-state NMR techniques.[8−11] In addition, the adsorbed structures of bone- and tooth-related molecules ranging from simple ions and small organic molecules to whole proteins on HAP surfaces have been intensively studied both experimentally and theoretically.[12−18] Despite being an important component of HAP−adsorbate studies, the molecular-level structures of HAP surfaces have been less studied and often overlooked. In particular, knowledge of the surface structures[19−23] under aqueous environments is crucial for understanding biological processes taking place at mineral/body fluid interfaces, such as bone resorption/mineralization and dental caries formation. Importantly, on the molecular level, these processes are governed by crystal growth and retraction along molecular steps.[24−27] Previously, atomic force microscopy techniques have been used to characterize the kinetics of HAP nucleation and dissolution by direct observation of molecular steps.[28−30] However, a detailed characterization of steps on hydroxyapatite surfaces is relatively unexplored. Here, we report on the orientations of individual molecular steps under both static conditions in pure water and also under dynamic dissolution conditions in acidic buffers using atomic force microscopy (AFM). We found that molecular steps parallel to the elongated axes of HAP crystals ([001] direction) and those angled approximately 54° from the elongated axis are not only energetically favorable but also kinetically dominant under dissolution conditions.

*To whom correspondence should be addressed. E-mail: leesw@berkeley.edu.

(1) Elliott, J. C., *Structure and Chemistry of the Apatites and Other Calcium Orthophosphates*; Elsevier: Amsterdam, 1994; pp xiii, 387.
(2) Kay, M. I.; Young, R. A.; Posner, A. S. *Nature* **1964**, *204*, 1050-&.
(3) Hunter, G. K.; Goldberg, H. A. *Proc. Natl. Acad. Sci. U.S.A.* **1993**, *90*, 8562–8565.
(4) Romberg, R. W.; Werness, P. G.; Riggs, B. L.; Mann, K. G. *Biochemistry* **1986**, *25*, 1176–1180.
(5) Hoang, Q. Q.; Sicheri, F.; Howard, A. J.; Yang, D. S. C. *Nature* **2003**, *425*, 977–980.
(6) Capriotti, L. A.; Beebe, T. P.; Schneider, J. P. *J. Am. Chem. Soc.* **2007**, *129*, 5281–5287.
(7) Palmer, L. C.; Newcomb, C. J.; Kaltz, S. R.; Spoerke, E. D.; Stupp, S. I. *Chem. Rev.* **2008**, *108*, 4754–4783.
(8) Goobes, G.; Goobes, R.; Schueler-Furman, O.; Baker, D.; Stayton, P. S.; Drobny, G. P. *Proc. Natl. Acad. Sci. U.S.A.* **2006**, *103*, 16083–16088.
(9) Shaw, W. J.; Long, J. R.; Campbell, A. A.; Stayton, P. S.; Drobny, G. P. *J. Am. Chem. Soc.* **2000**, *122*, 7118–7119.
(10) Shaw, W. J.; Campbell, A. A.; Paine, M. L.; Snead, M. L. *J. Biol. Chem.* **2004**, *279*, 40263–40266.
(11) Reid, D. G.; Duer, M. J.; Murray, R. C.; Wise, E. R. *Chem. Mater.* **2008**, *20*, 3549–3550.
(12) Cardenas, M.; Valle-Delgado, J. J.; Hamit, J.; Rutland, M. W.; Arnebrant, T. *Langmuir* **2008**, *24*, 7262–7268.
(13) Fleisch, H.; Russell, R. G. G.; Francis, M. D. *Science* **1969**, *165*, 1262−1264.
(14) Vitha, T.; Kubicek, V.; Hermann, P.; Koar, Z. I.; Wolterbeek, H. T.; Peters, J. A.; Lukes, I. *Langmuir* **2008**, *24*, 1952–1958.
(15) Filgueiras, M. R. T.; Mkhonto, D.; de Leeuw, N. H. *J. Cryst. Growth* **2006**, *294*, 60–68.
(16) Makrodimitris, K.; Masica, D. L.; Kim, E. T.; Gray, J. J. *J. Am. Chem. Soc.* **2007**, *129*, 13713–13722.
(17) Habelitz, S.; Kullar, A.; Marshall, S. J.; DenBesten, P. K.; Balooch, M.; Marshall, G. W.; Li, W. *J. Dental Res.* **2004**, *83*, 698–702.
(18) Wang, L. J.; Nancollas, G. H. *Chem. Rev.* **2008**, *108*, 4628–4669.
(19) Park, C. Y.; Fenter, P.; Zhang, Z.; Cheng, L. W.; Sturchio, N. C. *Am. Mineral.* **2004**, *89*, 1647–1654.
(20) Pareek, A.; Torrelles, X.; Rius, J.; Magdans, U.; Gies, H. *Phys. Rev. B* **2007**, *75*, 035418.
(21) Astala, R.; Stottt, M. J. *Phys. Rev. B* **2008**, *78*, 075427.
(22) Sato, K.; Kogure, T.; Iwai, H.; Tanaka, J. *J. Am. Ceram. Soc.* **2002**, *85*, 3054–3058.
(23) Bertinetti, L.; Tampieri, A.; Landi, E.; Ducati, C.; Midgley, P. A.; Coluccia, S.; Martra, G. *J. Phys. Chem. C* **2007**, *111*, 4027–4035.
(24) Stephenson, A. E.; DeYoreo, J. J.; Wu, L.; Wu, K. J.; Hoyer, J.; Dove, P. M. *Science* **2008**, *322*, 724–727.
(25) De Yoreo, J. J.; Vekilov, P. G. *Biomineralization* **2003**, *54*, 57–93.
(26) Gratz, A. J.; Manne, S.; Hansma, P. K. *Science* **1991**, *251*, 1343–1346.
(27) Onuma, K.; Ito, A. *Chem. Mater.* **1998**, *10*, 3346–3351.
(28) Onuma, K.; Ito, A.; Tateishi, T.; Kameyama, T. *J. Cryst. Growth* **1995**, *154*, 118–125.
(29) Kwon, K. Y.; Wang, E.; Chung, A.; Chang, N.; Saiz, E.; Choe, U. J.; Koobatian, M.; Lee, S. W. *Langmuir* **2008**, *24*, 11063–11066.
(30) Kwon, K. Y.; Wang, E.; Chung, A.; Chang, N.; Lee, S. W. *J. Phys. Chem. C* **2009**, *113*, 3369–3372.

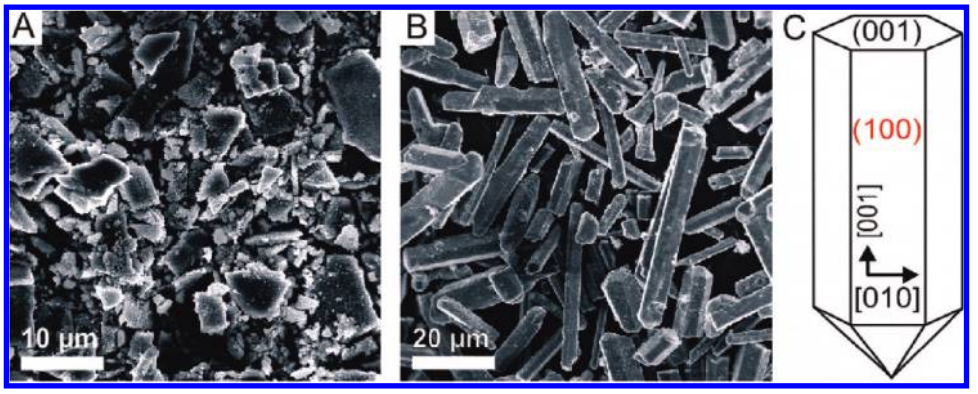

Figure 1. (A, B) SEM image of polycrystalline HAP powders (A) and HAP single crystals (B) after heating. (C) Model of a HAP crystal. Crystallographic axes and surfaces are defined.

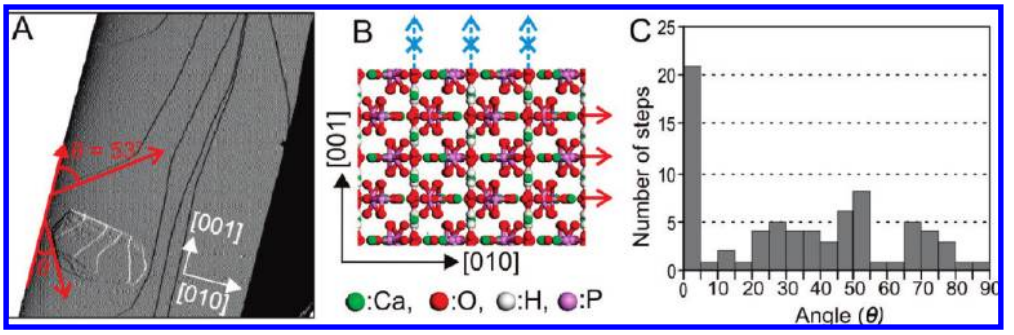

Figure 2. (A) AFM (deflection) image of a HAP (100) surface. (B) Surface symmetry of HAP (100) surfaces. Existence of mirror planes across the [010] directions and absence of mirror planes across the [001] directions indicated by red and blue arrows, respectively (Ca, green; O, red; H, white; P, purple). (C) Angular distribution of molecular steps on (100) surfaces.

Single-crystal HAP was synthesized by a molten salt synthesis method.[31] Scanning electron microscopy (SEM) shows the random morphology of the initial HAP powder before heating (Figure 1A). After heating (~1100 °C), the HAP powder transformed into crystalline HAP whiskers (Figure 1B). The details of the synthesis and XRD data of HAP whiskers were previously reported.[29] The resulting HAP crystals are hexagonal rods elongated along their *c* axis ([001] direction) and mainly expose six equivalent (100)-like surfaces (Figure 1B,C).

We characterized the various molecular steps found on HAP (100) surfaces by the measurement of their orientations and populations using AFM (Figure 2A). Before discussing the angles of individual steps, we will first note the symmetry of the HAP (100) surface. HAP is known to belong to the $P6_3/m$ or $P2_1/b$ space group.[2,32] On the basis of its (100) surface structure, there is mirror symmetry across the [010] direction but not about the [001] direction (Figure 2B). Experimentally, the elongated axis can be defined on the basis of the edges apparent in AFM images; however, absolute crystallographic directions cannot be defined because the [010] direction is indistinguishable from the $[0\bar{1}0]$ direction. Because of this ambiguity, for each sample surface, axes were consistently defined on the AFM images such that the [001] direction pointed upward and the [010] direction pointed toward the right as shown in Figure 2A. Therefore, the orientation of individual steps on (100) surfaces was assigned by the measurement of the acute angle (θ) between the elongation direction of the crystal and the step line (Figure 2A). By analyzing more than 50 HAP surfaces (Figure 2C), we found that the most dominantly observed steps are parallel to the [001] direction ($\theta \approx 0°$). Steps parallel to the [011] or $[0\bar{1}1]$ direction ($\theta \approx 54°$) have the second largest population.

On the basis of Gibbs−Wulff theorem, the shape of HAP crystals prepared under thermodynamic control can be used to determine the relative surface free energies of crystal facets.[33,34] It is proposed that the crystals tend to minimize the overall surface free energy for a given volume. In addition, the growth rates of individual facets are determined by relative surface free energies where facets having a higher surface free energy have a faster growth rate. Hence, the resulting crystal is mainly covered by surfaces with slower growth rates and correspondingly smaller surface free energies. Just as relative surface areas can be used to estimate relative surface energies, the population of specific step orientations relative to others on the surfaces of crystals formed under thermodynamic control can provide insight into their relative step energies. Because HAP crystals used in this study are prepared by a phase transition at elevated temperature, HAP's step orientations and populations are significantly determined by the energetics of individual steps. Therefore, on the basis of our observations, we conclude that steps with $\theta \approx 0°$ and 54° are energetically favorable compared to other step orientations on (100) HAP surfaces.

The energetically favorable step orientations observed on (100) HAP surfaces are also dominantly expressed during dissolution. Figure 3A shows an AFM image of a (100) surface in deionized water where two pits with approximately 5 nm depth are visible within the flat terrace regions. Noticeably, none of the steps enclosing these two pits have $\theta = 0$ or 54° (Figure 3B). We

(31) Tas, A. C. *J. Am. Ceram. Soc.* **2001**, *84*, 295–300.
(32) Elliott, J. C.; Mackie, P. E.; Young, R. A. *Science* **1973**, *180*, 1055–1057.
(33) Gibbs, J. W.; Bumstead, H. A.; Van Name, R. G.; Longley, W. R.; Lawrence, E. O. *The Collected Works of J. Willard Gibbs*. 2nd ed.; Longmans Green and Co.: New York, 1928; p 2 v.
(34) Wulff, G. *Z. Krystallogr. Mineral.* **1901**, *34*, 449–530.

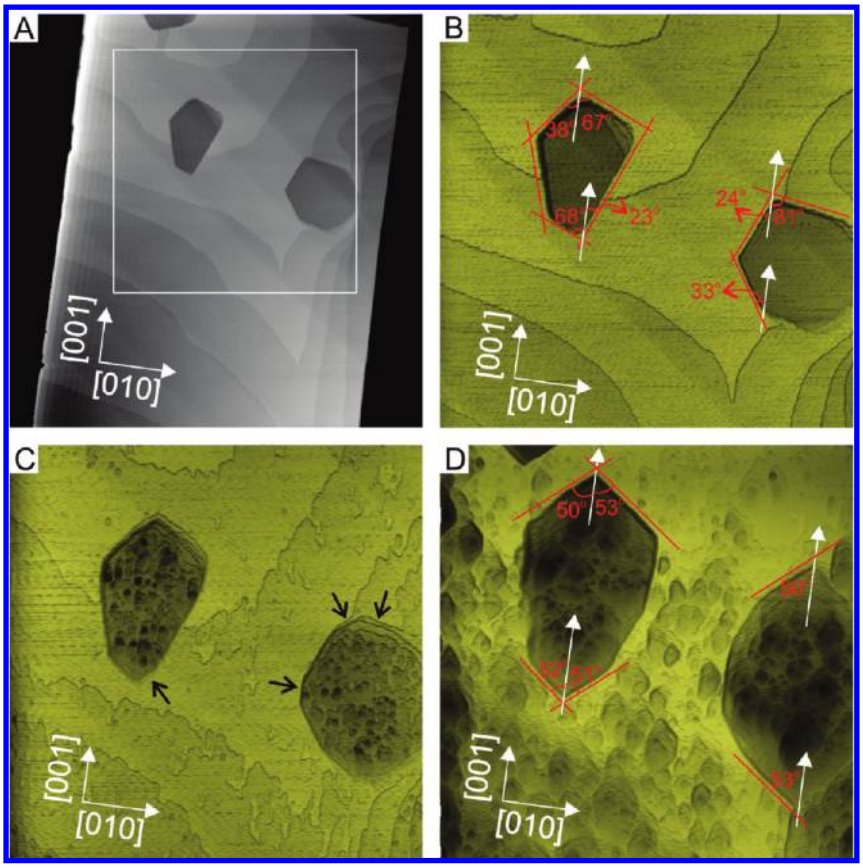

Figure 3. (A) AFM image of a HAP (100) surface ($5.0 \times 5.0\ \mu m^2$). Pentagon- (left) and hexagon-shaped (right) pits are embedded in the terrace. (B) White boxed region in A in deionized water ($3.0 \times 3.0\ \mu m^2$). Acute angles against the [001] direction are designated. (White arrows in the pits represent the [001] direction.) (C) AFM image 2 h after the injection of pH 6.00 acidic buffer. New step orientations are evolved during dissolution (black arrows). (D) Change in pit shape (11 h later). The orientation of newly evolved steps is approximately parallel to either the [001] direction ($\theta = 0$ °) or the [011] direction ($\theta = 54$ °).

followed the dissolution of this surface under the constant flow of an acidic buffer (pH 6, 10 mM citrate). Similar to our previous studies,[29] dissolution proceeded by the stochastic formation of new etch pits and continued by the retraction of their steps with a quantized height of 0.83 nm, which were previously observed in both dissolution and nucleation processes[28−30] (Movie S1). Compared to the initial step orientations that defined the pits prior to the addition of acidic buffer (Figure 3B), new step orientations began to be generated during the dissolution process (arrows in Figure 3C). Figure 3D shows an AFM image 11 h after the injection of acidic buffer in which all of the initial step orientations shown in Figure 3B have almost disappeared and pits with approximately hexagonal shape are enclosed by newly formed steps. The orientations of steps formed during dissolution are determined by the kinetics of individual step retraction. Steps with faster retraction velocities have shorter lengths or disappear altogether whereas steps with relatively slow retraction velocities form longer edges. Therefore, the step orientations that evolved have slower retraction velocities than the initial step orientations had. Most importantly, the orientations of the new steps enclosing the hexagonal pits match the major step orientations observed on the HAP (100) surface ($\theta = 0$ and 54°) prepared by molten salt synthesis (Figure 3D).

After the initial step orientations were superseded by those with slower retraction velocities, enlargement of the hexagonal pits proceeded by retraction of four crystallographically distinct steps. The model of the step orientations enclosing the hexagonal pits are shown in Figure 4A. Because of the aforementioned surface asymmetry, the steps with $\theta = 54°$ can be divided into two pairs of crystallographically equivalent steps: ($[011]_+$ and $[0\bar{1}1]_+$) and ($[011]_-$ and $[0\bar{1}1]_-$). Similarly, two crystallographically nonequivalent steps ($[001]_+$ and $[001]_-$) exist parallel to the [001] direction. We determined individual step velocities using sequential AFM images by measuring step displacements over a given time (Figure 4B). Step velocities with $[011]_-$ or $[0\bar{1}1]_-$, $[001]_-$, $[011]_+$ or $[0\bar{1}1]_+$, and $[001]_+$ directions are 5.1, 4.6, 3.0, and 2.2 pm/s, respectively. Consistent with the behavior of etch pit dissolution initiated at defects sites, although the hexagonal pit shape is approximately symmetric across the [001] direction, we found that the retraction velocities of steps on one side (− annotation in Figure 4A) are almost 2 times faster than their counterparts on the other side (+ annotation in Figure 4A), as shown in Figure 4C.

There are a number of factors that influence the relative step retraction velocity. Because the dissolution rate increases as the solution pH decreases,[35−37] two factors in particular are expected to play important roles in determining relative step velocities: (i) how easily a step is attacked by protons and (ii) how much the protonation of specific steps can lower the activation energy of calcium phosphate bond breaking. Regardless of these plausible kinetic variables affecting step velocity during dissolution, we found that the step orientations that evolve during dissolution are the same as the dominant step orientations found on HAP crystal surfaces prepared under thermodynamic

(35) Christoffersen, J.; Christoffersen, M. R. *J. Cryst. Growth* **1982**, *57*, 21–26.
(36) Tang, R. K.; Nancollas, G. H.; Orme, C. A. *J. Am. Chem. Soc.* **2001**, *123*, 5437–5443.
(37) Brady, B. H. G.; Mapper, D. H.; Smythe, B. M. *Nature* **1966**, *212*, 77−78.

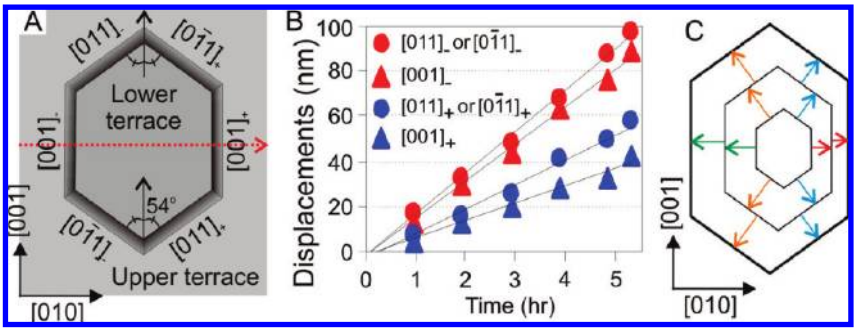

Figure 4. (A) Model of a hexagonal pit. Four crystallographically distinct steps are (i) $[001]_+$, (ii) $[001]_-$, (iii) $[011]_+$ or $[0\bar{1}1]_+$, and (iv) $[011]_-$ or $[0\bar{1}1]_-$. (B) Step retraction displacements vs time. Step velocities with $[011]_-$ or $[0\bar{1}1]_-$, $[001]_-$, $[011]_+$ or $[0\bar{1}1]_+$, and $[001]_+$ are 5.1, 4.6, 3.0, and 2.2 pm/s, respectively. (C) Schematic of the evolution of hexagonal etch pits. Four differently colored arrows represent relative step velocities.

control. On the basis of these results, we conclude that the dissolution kinetics of individual steps is chiefly dependent on their thermodynamic stability where steps parallel to the [001] and [011] (or $[0\bar{1}1]$) directions are both energetically and kinetically favored.

Acknowledgment. This work was supported by a National Science Foundation Early Career Development Award (DMR-0747713), start-up funds from the Nanoscience and Nanotechnology Institute at the University of California, Berkeley, and the Laboratory Directed Research and Development Fund from the Lawrence Berkeley National Laboratory.

Supporting Information Available: A dissolution AFM movie. This material is available free of charge via the Internet at http://pubs.acs.org.